Received July 1, 2017, accepted August 1, 2017, date of publication August 4, 2017, date of current version October 25, 2017.

Digital Object Identifier 10.1109/ACCESS.2017.2736019

Imaging of Lung Structure Using Holographic Electromagnetic Induction

LULU WANG[1,2], (Member, IEEE), AND AHMED M. AL-JUMAILY[2]
[1]School of Instrument Science and Opto-Electronics Engineering, Hefei University of Technology, Hefei 230009, China
[2]Institute of Biomedical Technologies, Auckland University of Technology, Auckland 1010, New Zealand

Corresponding author: Lulu Wang (luluwang2015@hfut.edu.cn)

This work was supported in part by the National Natural Science Foundation of China (NSFC) under Grant 61701159, in part by the Natural Science Foundation of Anhui Province under Grant 101413246, in part by the Foundation for Oversea Master Project from the Ministry of Education, China, under Grant 2160311028, in part by the start-up funding from the Hefei University of Technology under Grant 407037164, and in part by the Institute of Biomedical Technologies, Auckland University of Technology, New Zealand.

ABSTRACT Early lung cancer detection with suitable treatment can significantly reduce cancer-related death rates. This paper presents a single frequency holographic electromagnetic induction (HEI) imaging method for small lung tumor detection in human thorax models. A numerical system is developed to study the feasibility of early lung tumor detection. The system includes various realistic tumors within a thorax model and a HEI measurement model. Simulation results show that various arbitrary shaped lung tumors with random sizes and locations can be identified in the thorax images. The proposed protocol has the potential for the further instantiation of lung structure.

INDEX TERMS Electromagnetic induction imaging, magnetic induction tomography, antenna array, lung cancer, dielectric properties.

I. INTRODUCTION

Lung cancer is a common disease with a high death rate in the United States and worldwide [1]. Diagnosis of early stage lung cancer with suitable treatment could increase the 5-year survival rate [2]. To reduce mortality, various medical screening methods such as computed tomography (CT), chest radiography, MRI, ultrasound, and magnetic induction tomography (MIT) have been intensively investigated. However, most of them are expensive and not sensitive enough for detecting early stage lung tumors [3]. CT detects more early stage lung tumors than conventional radiography, but it is relatively expensive and not very helpful in reducing mortality [4]. Improvement in sensitivity with low cost is considered as a first step in early cancer detection.

MIT has received many attentions worldwide [5] due to the fact it is cost effective and less complicated than other methods. In principle, it aims at mapping the electromagnetic properties (conductivity, permittivity, and permeability) distribution of a target object. If a target object is placed in a MIT system, an array of inductive coils arranged around the object induce magnetic field on the object. The spatial distribution of the magnetic field and the mutual coupling between the coils is altered by the object [6]. Thus, the scattered field from this object (consists of voltage and phase information) is then measured and the produced data can be used to reconstruct the object.

MIT has been used in numerous areas, including geological exploration, non-destructive evaluations, foreign material monitoring and biomedical imaging [7]–[20]. For biomedical imaging applications, various MIT approaches have been investigated with particular focus on imaging lung [21], [22], brain [23], [24], heart [25]–[27], liver tissue [28], [29] and biological tissues [30], [31]. Gabriel et al. [32]–[34] have intensively investigated several types of human tissues over a wide frequency range. The simplicity of characterizing passive electrical properties of the biological tissues offers an alternative approach for biological tissue imaging. Al-Zeibak and Saunders [35] was the first to investigate the MIT theory for imaging of a biological object in order to distinguish between fat and water-bearing fat free tissues. However, MIT industrial processing is still challenging. It has not been extensively investigated in clinical environments because of the limited image resolution and it has not met the standards for widespread commercialization [6]. Thus, the simplicity of MIT and its low cost offer an attractive choice of medical imaging.

Holography techniques have recently been applied in the biomedical imaging field [36], [37]. The authors previously

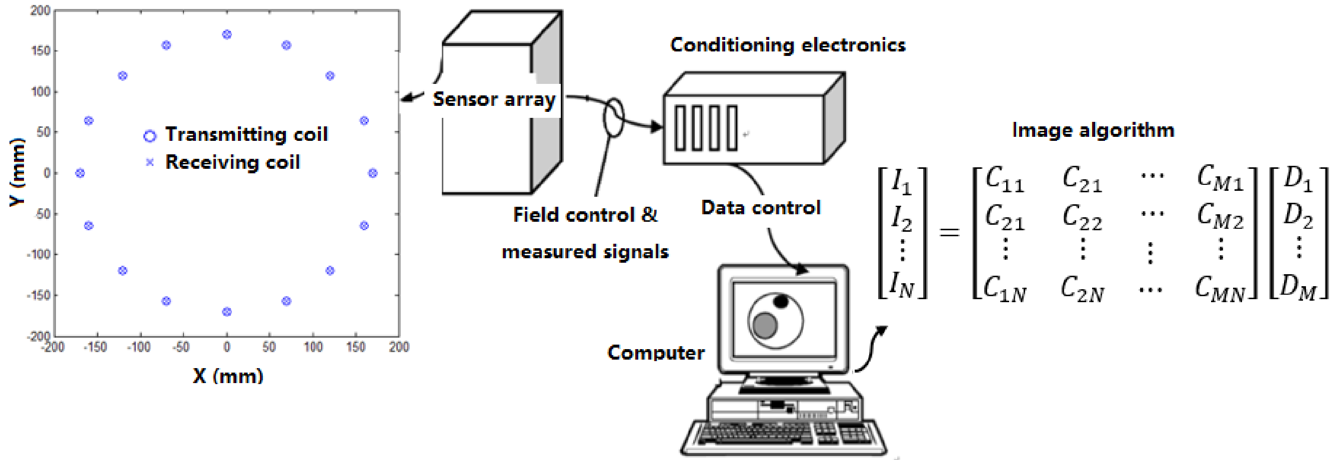

FIGURE 1. HEI imaging system measurement setup.

proposed a holographic electromagnetic induction (HEI) method for imaging a dielectric object with a particular focus on brain stroke detection [38]. This paper aims at studying the feasibility of lung tumor detection in realistic human thorax models using a single frequency HEI based method. A numerical system, including a HEI measurement model and various human thorax models, is developed to investigate the theory of HEI and system setups. The detectability of small lung tumors with HEI is evaluated through numerical simulations.

The manuscript is organized as follows. Section II introduces HEI theory and system setups. Section III describes the development of the numerical system that includes various thorax models, and results are presented in Section IV. The discussion and conclusion are given in Section V.

II. THEORY

Figure. 1 displays the single frequency HEI approach for early lung tumor detection, which contains a cylindrical tank with 16 transceiver coils. Each coil works as transmitter and detector. The thorax model is located in the middle of the tank and is energized with a magnetic field generated by coils located outside of the tank wall. During data collection, the transmitting coils transmit electromagnetic (EM) signals into the thorax, and the receiving coils measure the scattered magnetic fields from the thorax. A reconstructed image of the thorax model can be obtained from the measurement data.

Referring to Figure. 2, a point Q is located within the thorax model, the complex visibility data for any two coils can be calculated using the measured scatted magnetic field [39]:

$$\overrightarrow{V_{i,j}} = \langle \overrightarrow{H}_{scat}(\overrightarrow{r_i}) \cdot \overrightarrow{H}^*_{scat}(\overrightarrow{r_j}) \rangle \tag{1}$$

Where the two coils located at $\overrightarrow{r_i}$ and $\overrightarrow{r_j}$, $\langle\rangle$ means the time average, $\overrightarrow{H}_{scat}$ and $\overrightarrow{H}^*_{scat}$ are the scattered magnetic field and the conjugate complex of the scattered electromagnetic field, respectively. For N coils, the total complex visibility data is $\overrightarrow{V} = \sum_i^N \overrightarrow{V_{i,j}}, N \geq 3, i \neq j$.

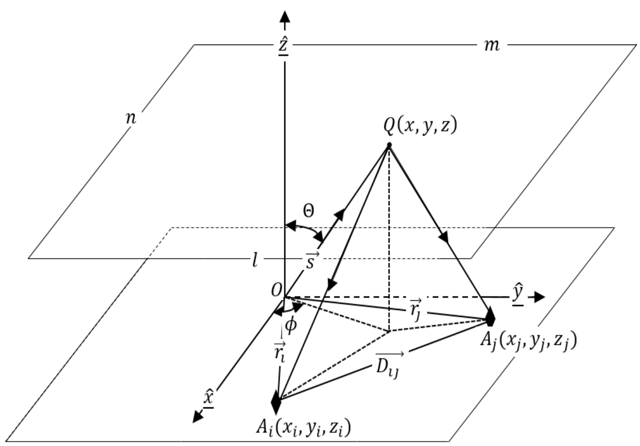

FIGURE 2. HEI measurement by any pair of coils.

Define the thorax intensity:

$$I(\vec{s}) = \left(\frac{j\omega\mu_0}{4\pi}\right)^2 |\sigma(s) + j\omega\varepsilon_0\varepsilon_r'|^2 \overrightarrow{H_T}(\vec{s}) \cdot \overrightarrow{H_T^*}(\vec{s}\,') \tag{2}$$

Where ω is angular frequency, μ_0 and ε_0 are permeability and permittivity of free space, σ and $\varepsilon_r(= \varepsilon_r' - j\varepsilon_r'')$ are conductivity and complex relative permittivity of thorax, respectively.

If all detectors are positioned on a 2D plane (same height), then define line integral:

$$\tilde{I}(l, m) = \int_s \frac{I(s, l, m)}{\sqrt{1 - l^2 - m^2}} ds \tag{3}$$

Where $l = sin\theta cos\phi$ and $m = sin\theta sin\phi$ (see Figure. 2).

The complex visibility data becomes:

$$V(u_{ij}, v_{ij}) = \int_l \int_m \int_n \frac{I(s, l, m)}{\sqrt{1 - l^2 - m^2}} e^{(-j2\pi\Phi_{ij})} dldmds \tag{4}$$

Where $\Phi_{ij} = u_{ij}l + v_{ij}m$, $u_{ij} = (\overrightarrow{x_j} - \overrightarrow{x_i})/\lambda_0$ and $v_{ij} = (\overrightarrow{y_j} - \overrightarrow{y_i})/\lambda_0$, λ_0 indicates the wavelength of free space.

A 2D image can be reconstructed:

$$\tilde{I}(l,m) = \int\int V(u,v)\, e^{j2\pi(u_{ij}l+v_{ij}m)}dudv \tag{5}$$

III. MATH NUMERICAL SYSTEM

A numerical system (as shown in Figure. 1) is developed to investigate the feasibility of HEI for lung tumor detection under MATLAB environment. The system is made of 16 circular coils (2cm) and placed 2cm above the bottom. The electric current density generated from transmitter is 1A/m^2. To calculate voltages, finite element approach is used and the measured region is divided into triangular meshes. The working frequency is 2MHz.

A. FORWARD MODEL

The excitation current density $\overrightarrow{J_s}$ can be simulated by:

$$\overrightarrow{J_s} = \nabla \times \left(\mu_0^{-1}\nabla \times \overrightarrow{A}\right) + j\omega\sigma\overrightarrow{A} \tag{6}$$

Where ∇ is the divergence operator, $\overrightarrow{A}$ is the magnetic potential vector. Equation (6) can be rewritten from Maxwell's formulas by calculating the total electric field $\overrightarrow{E} = j\omega\overrightarrow{A} - \nabla\Omega$, Ω is the electric scalar potential.

B. BACKWARD MODEL

For any receiving coils, the scattered field from the thorax can be modeled by using the follow expression [40]:

$$\overrightarrow{H}_{scat}(\overrightarrow{r_0}) = \frac{-j}{4\pi\omega\mu_0}\int_V [(\overrightarrow{J_s}\cdot\nabla)\times\nabla + k_0^2\overrightarrow{J_M} + j\omega\mu_0\overrightarrow{J_S}\nabla]G(\overrightarrow{r},\overrightarrow{r_0})dV \tag{7}$$

Where $\overrightarrow{r_0}$ is the distance from origin to the target point, $\overrightarrow{r}$ is the distance from origin to the target object. k_0 means prorogation constant of free space, $\overrightarrow{J_s} = j\omega\varepsilon_0(\varepsilon_r - 1)\overrightarrow{E}$, $\overrightarrow{J_M} = j\omega\mu_0(\mu_r - 1)\overrightarrow{H_T}$, ε_r is the relative permittivity of thorax. The total magnetic field can be computed by $\overrightarrow{H_T} = \overrightarrow{H}_{inc} + \overrightarrow{H}_{scat}$.

Using the following formula to calculate the magnetic field:

$$\overrightarrow{H}_{scat}(\overrightarrow{r_0}) = \frac{k_0^2}{4\pi}\int_V [(a\overrightarrow{H} + b(\overrightarrow{H}\cdot\underline{\hat{r}})\underline{\hat{r}})]G(\overrightarrow{r},\overrightarrow{r_0})dV \tag{8}$$

Where $\underline{\hat{r}}$ is unit vector from origin to the object, $a = \mu_r\varepsilon_r - \frac{j(\mu_r-1)}{k_0R}(1 - \frac{j}{k_0R})$, $b = (\mu_r - 1)(-1 + \frac{3j}{k_0R} + \frac{3}{(k_0R)^2})$, R is the distance between source and the object, a and b are proportional to $1/R^2$(i.e. $k_0R \ll 1$). Hence $k_0^2a \cong -(\mu_r - 1)/R^2$ and $k_0^2b \cong 3(\mu_r - 1)/R^2$.

Equation (8) changes to:

$$\overrightarrow{H}_{scat}(\overrightarrow{r_0}) = \frac{1}{4\pi}\int_V \frac{\mu_r - 1}{R^2} \times [-\overrightarrow{H} + 3(\overrightarrow{H}\cdot\underline{\hat{r}})\underline{\hat{r}})]G\left(\overrightarrow{r},\overrightarrow{r_0}\right)dV \tag{9}$$

If the frequency is relatively small, equation (9) is valid, for example the target object is much smaller compared to the wavelength. This means no frequency dependence. Therefore, a quasi-static approximation emerges as the dominant term when magnetic materials are introduced.

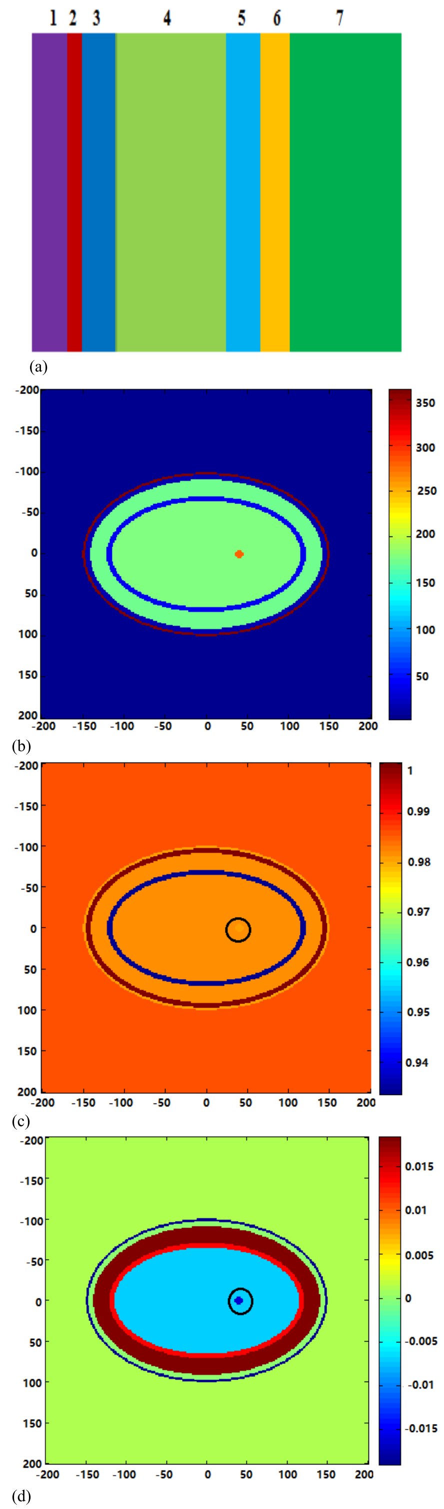

FIGURE 3. **(a) Multilayer thorax model, 1: air, 2: skin (3mm), 3: fat (6mm), 4: muscle (20mm), 5: bone, (6mm) 6: tumor (10mm), 7: lung tissue. (b) Thorax model under test; (c) Reconstructed image (real-part). (d) Reconstructed image (imaginary-part).**

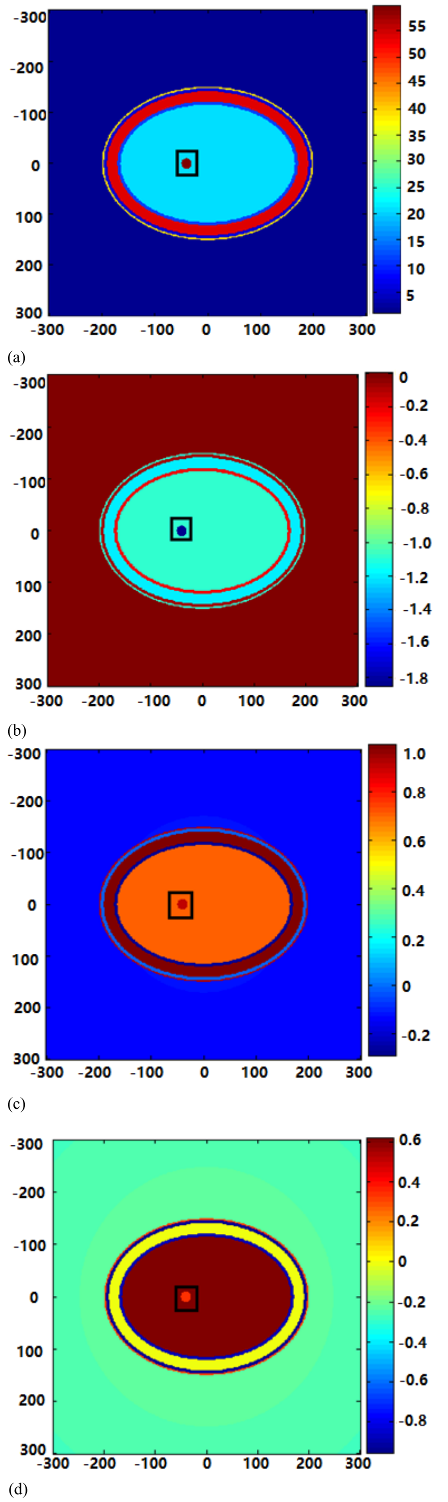

FIGURE 4. **(a) 2D view of permittivity of thorax model II. (b) 2D view of conductivity of thorax II. (c) Reconstructed image of thorax model II (real-part). (d) Reconstructed image of thorax model II (imaginary-part).**

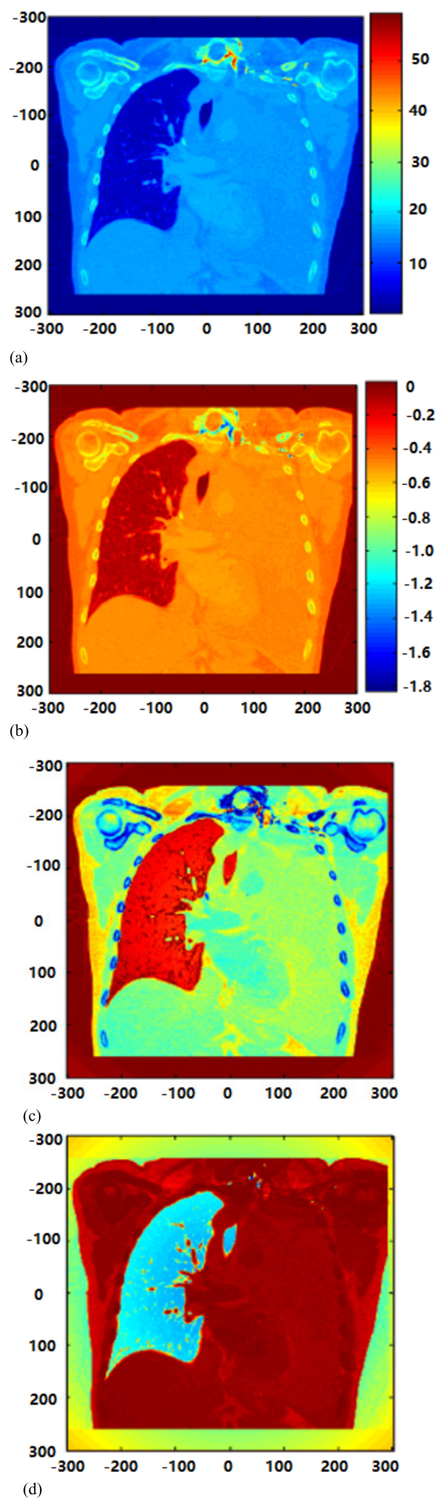

FIGURE 5. **(a) 2D view of permittivity of thorax model III. (b) 2D view of conductivity of thorax III. (c) Reconstructed image of thorax model III (real-part). (d) Reconstructed image of thorax model III (imaginary-part).**

Born Approximation can be applied to evaluate (9) when performing the forward model [41]. Thus, the magnetic field inside the thorax can be modeled approximately as the incident field that exists at the same location but without the thorax presented in the imaging domain. The excitation coil is used to generate incident field.

C. THORAX MODELS

Three human thorax models are developed using the published dielectric properties of thorax tissues in order to evaluate the detectability of lung tumor [42]. Thorax model I ($100 \times 50mm^2$) and thorax model II ($400 \times 250 \times 70mm^3$) are made of 6 tissues: skin, fat, muscle, bone, lung tissue and tumor (10mm circle in Model I and 10mm sphere in Model II).

Thorax model III is developed based on CT images that were obtained with a 1.25mm slice thickness [43]. The CT data contained 42 images and each image has 512×512 elements. MATLAB software is applied to import all CT images to construct a realistic 3D thorax phantom, and 2D thorax models are developed by considering a single slice of CT-based thorax model.

IV. RESULTS

To investigate the HEI theory and system configurations, several simulations were performed using the developed thorax models. All thorax models were measured in millimeter (mm) as shown in the figures.

Figure. 3 shows the original and reconstructed images of thorax model I at a frequency of 10MHz. A small lung tumor (circled in black) is displayed in the reconstructed images. Figure. 4 displays the original and reconstructed images of thorax model II. The structure of the thorax tissues and small sphere lung tumor (10mm in diameter, squared in black) can be clearly identified in the reconstructed images.

Figure. 5(a)-(b) display 2D views of permittivity and conductivity of model III. Figure. 5(c) and Figure. 5(d) shows the reconstructed images of thorax model III. The structure of the lung and various small lung tumors with arbitrary shapes, sizes and locations can be identified in the reconstructed images.

Each image in Figures 4 and 5 contains 512×512 elements. Color bars plot dielectric properties of the thorax model in original images and plot scale signal energy in the reconstructed images.

V. CONCLUSION

This study investigated the HEI approach for small lung tumor detection and the theory has been validated through various realistic human thorax models. It was found that various arbitrary shaped lung tumors with random sizes and locations can be identified. Results showed that HEI has potential for investigating characterization and structure of the lung tissue. The proposed framework provides crucial priority information that can be exploited to improve the capabilities of MIT diagnostics methods.

The HEI image quantity is proportional to the dielectric properties contrast; it is much simpler compared to existing MIT approaches because heavy computation work of dielectric properties is not required. Results demonstrated that the proposed work has the potential to become a useful tool for computer visualization and optimization of the HEI system before it can be implemented and validated in practice.

REFERENCES

[1] *Cancer Fact Sheet*, WHO Media Centre, Geneva, Switzerland, Feb. 2017.
[2] N. Altorki, M. Kent, and M. Pasmantier, "Detection of early-stage lung cancer: Computed tomographic scan or chest radiograph?" *J. Thoracic Cardiovascular Surgery*, vol. 121, no. 6, pp. 1053–1057, 2001.
[3] M. E. Deffebach and L. Humphrey, "Lung cancer screening," *Surgical Clin. North Amer.*, vol. 95, no. 5, pp. 967–978, 2015.
[4] N. Chalmers and J. J. K. Best, "The significance of pulmonary nodules detected by CT but not by chest radiography in tumour staging," *Clin. Radiol.*, vol. 44, no. 6, pp. 410–412, 1991.
[5] H. Griffiths, "Magnetic induction tomography," *Meas. Sci. Technol.*, vol. 12, no. 8, pp. 1126–1131, 2001.
[6] A. Korzhenevsky and S. Sapetsky, "Visualisation of the internal structure of extended conducting objects by magnetoinduction tomography," *Bull. Russian Acad. Sci., Phys.*, vol. 65, no. 12, pp. 1945–1949, 2011.
[7] Z. Zakaria *et al.*, "Magnetic induction tomography: A review on the potential application in agricultural industry of Malaysia," *J. Agricult. Sci.*, vol. 5, no. 9, pp. 78–82, 2013.
[8] M. Han, X. Cheng, and Y. Xue, "Comparison with reconstruction algorithms in magnetic induction tomography," *Physiol. Meas.*, vol. 37, no. 5, p. 683, 2016.
[9] C. von Hebel *et al.*, "Three-dimensional imaging of subsurface structural patterns using quantitative large-scale multiconfiguration electromagnetic induction data," *Water Resour. Res.*, vol. 50, no. 3, pp. 2732–2748, 2014.
[10] H.-Y. Wei and M. Soleimani, "Hardware and software design for a national instrument-based magnetic induction tomography system for prospective biomedical applications," *Physiol. Meas.*, vol. 33, no. 5, p. 863, 2012.
[11] L. Ma, A. Hunt, and M. Soleimani, "Experimental evaluation of conductive flow imaging using magnetic induction tomography," *Int. J. Multiphase Flow*, vol. 72, no. 20, pp. 198–209, 2015.
[12] S. Teniou, M. Meribout, K. Al-Wahedi, A. Al-Durra, and E. Al-Hosani, "A near-infrared-based magnetic induction tomography solution to improve the image reconstruction accuracy in opaque environments," *IEEE Trans. Magn.*, vol. 49, no. 4, pp. 1361–1366, Apr. 2013.
[13] J. Wood *et al.*, "Effect of shielding conductivity on magnetic induction tomographic security imagery," *IEEE Trans. Magn.*, vol. 53, no. 4, Apr. 2017, Art. no. 4000406.
[14] L. Ma and M. Soleimani, "Critical evaluation of two phase low conductivity flow imaging using magnetic induction tomography," *J. Immunol.*, vol. 183, no. 7, pp. 4493–4501, 2014.
[15] G. Jin *et al.*, "A new method for detecting cerebral hemorrhage in rabbits by magnetic inductive phase shift," *Biosensors Bioelectron.*, vol. 52, no. 4, pp. 374–378, 2014.
[16] C. Deans, L. Marmugi, S. Hussain, and F. Renzoni, "Electromagnetic induction imaging with a radio-frequency atomic magnetometer," *Appl. Phys. Lett.*, vol. 108, no. 10, p. 103503, 2016.
[17] J. M. S. Caeiros and R. C. Martins, "An optimized forward problem solver for the complete characterization of the electromagnetic properties of biological tissues in magnetic induction tomography," *IEEE Trans. Magn.*, vol. 48, no. 12, pp. 4707–4712, Dec. 2012.
[18] H. Griffiths, W. R. Stewart, and W. Gough, "Magnetic induction tomography: A measuring system for biological tissues," *Ann. New York Acad. Sci.*, vol. 873, no. 1, pp. 335–345, 1999.
[19] M. Zhang and M. Soleimani, "A combined magnetic induction electrical capacitance tomography," *J. Invest. Dermatol.*, vol. 105, no. 3, pp. 329–333, 2014.
[20] L. L. Mariappan, G. Hu, and B. He, "Magnetoacoustic tomography with magnetic induction for high-resolution bioimepedance imaging through vector source reconstruction under the static field of MRI magnet," *Med. Phys.*, vol. 41, no. 2, p. 022902, 2014.
[21] D. Gürsoy and H. Scharfetter, "Feasibility of lung imaging using magnetic induction tomography," in *World Congress on Medical Physics and Biomedical Engineering*. Munich, Germany: Springer, 2009.
[22] Z. Zakaria *et al.*, "Advancements in transmitters and sensors for biological tissue imaging in magnetic induction tomography," *Sensors*, vol. 12, no. 6, pp. 7126–7156, 2012.
[23] R. Liu, Y. Li, F. Fu, F. You, X. Shi, and X. Dong, "Time-difference imaging of magnetic induction tomography in a three-layer brain physical phantom," *Meas. Sci. Technol.*, vol. 25, no. 6, p. 065402, 2014.
[24] Z. Xu, H. Luo, W. He, C. He, X. Song, and Z. Zahng, "A multi-channel magnetic induction tomography measurement system for human brain model imaging," *Physiol. Meas.*, vol. 30, no. 6, p. S175, 2009.

[25] L. Marmugi and F. Renzoni, "Optical magnetic induction tomography of the heart," *Sci. Rep.*, vol. 6, Apr. 2016, Art. no. 23962.
[26] C. Deans, L. Marmugi, S. Hussain, and F. Renzoni, "Optical atomic magnetometry for magnetic induction tomography of the heart," *Proc. SPIE*, vol. 9900, Apr. 2016, Art. no. 99000F.
[27] R. Casañas *et al.*, "Measurement of liver iron overload by magnetic induction using a planar gradiometer: Preliminary human results," *Physiol. Meas.*, vol. 25, no. 1, pp. 315–323, 2004.
[28] G. Hu, E. Cressman, and B. He, "Magnetoacoustic imaging of human liver tumor with magnetic induction," *Appl. Phys. Lett.*, vol. 98, no. 2, p. 023703, 2011.
[29] A. Morris, H. Griffiths, and W. Gough, "A numerical model for magnetic induction tomographic measurements in biological tissues," *Physiol. Meas.*, vol. 22, no. 1, p. 113, 2001.
[30] X. Li, Y. Xu, and B. He, "Magnetoacoustic tomography with magnetic induction for imaging electrical impedance of biological tissue," *J. Appl. Phys.*, vol. 99, no. 6, p. 066112, 2016.
[31] H. Scharfetter, H. K. Lackner, and J. Rosell, "Magnetic induction tomography: Hardware for multi-frequency measurements in biological tissues," *Physiol. Meas.*, vol. 22, no. 1, p. 131, 2001.
[32] C. Gabriel, S. Gabriel, and E. Corthout, "The dielectric properties of biological tissues: I. Literature survey," *Phys. Med. Biol.*, vol. 41, no. 11, pp. 2231–2249, Nov. 1996.
[33] S. Gabriel, R. W. Lau, and C. Gabriel, "The dielectric properties of biological tissues: II. Measurements in the frequency range 10 Hz to 20 GHz," *Phys. Med. Biol.*, vol. 41, no. 11, pp. 2251–2269, Nov. 1996.
[34] S. Gabriel, R. W. Lau, and C. Gabriel, "The dielectric properties of biological tissues: III. Parametric models for the dielectric spectrumof tissues," *Phys. Med. Biol.*, vol. 41, no. 11, pp. 2271–2293, Nov. 1996.
[35] S. Al-Zeibak and N. H. Saunders, "A feasibility study of *in vivo* electromagnetic imaging," *Phys. Med. Biol.*, vol. 38, no. 1, p. 151, 1993.
[36] D. M. Sheen, D. H. Collins, T. E. Hall, D. L. Mcmakin, P. R. Gribble, and R. H. Severtsen, "Real-time wideband holographic surveillance system," U.S. Patent 5 557 283, Sep. 17, 1996.
[37] G. Tricoles and N. H. Farhat, "Microwave holography—Applications and techniques," *Proc. IEEE*, vol. 65, no. 1, pp. 108–121, Jan. 1997.
[38] L. Wang, "Electromagnetic induction holography imaging for stroke detection," *J. Opt. Soc. Amer. A, Opt. Image Sci. Vis.*, vol. 34, no. 2, pp. 294–298, 2017.
[39] R. Levanda and A. Leshem, "Synthetic aperture radio telescopes," *IEEE Signal Process. Mag.*, vol. 27, no. 1, pp. 14–29, Jan. 2010.
[40] L. Wang, A. M. Al-Jumaily, and R. Simpkin, "Imaging of 3-D dielectric 326 objects using far-field holographic microwave imaging technique," *Progr. Electromagn. Res. B*, vol. 61, pp. 135–147, Nov. 2014.
[41] M. Born, E. Wolf, and E. Hecht, *Principles of Optics: Electromagnetic Theory of Propagation, Interference and Diffraction of Light*. New York, NY, USA: Pergamon, 1975.
[42] Italian National Research Council. *An Internet Resource for the Calculation of the Dielectric Properties of Body Tissues in the Frequency Range 10 Hz–100 GHz*. Accessed on Aug. 10, 2017. [Online]. Available: http://niremf.ifac.cnr.it/tissprop
[43] *ELCAP Public Lung Image Database*. Accessed on Aug. 10, 2017. [Online]. Available: http://www.via.cornell.edu/lungdb.html

LULU WANG (M'12) received the B.E. (Hons.) degree from the Manukau Institute of Technology, New Zealand, and the M.E. (Hons.) and Ph.D. degrees from the Auckland University of Technology, New Zealand.

She is currently an Associate Professor with the School of Instrument Science and Opto-Electronics Engineering, Hefei University of Technology, Hefei, China. She is also an Honorary Research Officer with the Institute of Biomedical Technologies, Auckland University of Technology. She is the first author of over 35 papers in international journals and conference proceedings, including one ASME book and one book chapter on holographic microwave imaging in biomedical applications, and five patents. Her current research focuses on electromagnetic theory and imaging, respiratory diseases detection technologies, and medical devices. She is a member of several professional societies, including ASME, IEEE, AAAS, PSNZ, and IPNZ. She currently serves as a track co-organizer of Biomedical and Biotechnology and the Topic Organizer of Medical Devices, ASME International Mechanical Engineering Congress and Exposition.

AHMED M. AL-JUMAILY received the B.Sc. degree from the University of Baghdad, and the Ph.D. and M.Sc. degrees from The Ohio State University, Columbus, OH, USA. He is currently a Professor of biomechanical engineering and the Director of the Institute of Biomedical Technologies with the Auckland University of Technology, Auckland, New Zealand. He is a Fellow Member of the American Society of Mechanical Engineering (ASME), and a member of 11 more international professional societies. He has authored or co-authored over 300 papers in international journals and conference proceedings, including two ASME books on vibration and acoustics in biomedical applications and a third one on CPAP devices. He has supervised over 90 postgraduate students in biomedical applications, vibrations, biomechanics, and electroactive polymers. During his academic career, he has forged strong alliances between academia and industries, in particular in the medical devices area, which has resulted in many successful grants and contracts with companies and research organizations. His current research focuses on biomedical applications with particular interest in the application of vibration and acoustics to airways constriction therapies and artery non-invasive diagnostics.

He is an Editor of the *ASME Monograph Series-Biomedical and Nanomedical Technologies* and Editor-in-Chief of the *Journal of Biomedical Engineering and Technology*, and has been on the editorial and refereeing boards for several international journals.